Available online at www.sciencedirect.com
SCIENCE DIRECT®
Surface Science 600 (2006) L128–L133
SURFACE SCIENCE
www.elsevier.com/locate/susc

Surface Science Letters

Effect of electromagnetic interactions on plasmon excitations in silver particle ensembles

H.-M. Benia, N. Nilius *, H.-J. Freund

Fritz-Haber Institut der MPG, Faradayweg 4-6, D14195 Berlin, Germany

Received 11 August 2005; accepted for publication 16 March 2006
Available online 4 April 2006

Abstract

The optical properties of silver nano-particle ensembles are studied as a function of particle density by analyzing the light emission excited via electron injection from an STM tip. The particles are prepared with distinct dome and disk-like shapes on a Al_2O_3/NiAl(1 1 0) support. The particle density is varied over one order of magnitude by changing the Ag deposition temperature and the defect concentration in the oxide surface. With increasing density, a pronounced blue shift of the Ag plasmon mode is observed for ensembles of dome-like particles, whereas disk-like particles show relatively constant resonance energies. The observed evolution of plasmon energy as a function of particle density reflects the influence of electromagnetic interactions in the ensemble, as verified by model calculations.

Keywords: Silver particles; Photon emission spectroscopy; Scanning tunneling microscopy

Metal nano-particles have been subject of intensive studies in various research fields thanks to their special electromagnetic properties related to Mie-plasmon excitations [1]. Particularly, noble metal particles (e.g., Au and Ag) play a big role in several applications, such as surface-enhanced Raman spectroscopy [2], optical filters [3], plasmon waveguides [4], and photo-chemistry [5]. The electromagnetic response of a particle ensemble depends on size and shape of the particles, the surrounding medium, and the particle–particle interactions determined by the mean particle density on the surface [1]. Optimal performance of future devices based on plasmon excitations can only be ensured when the influence of each of these parameters is fully explored and independently adaptable to the demands of a specific application.

The choice of a suitable preparation method is crucial for the fabrication of ensembles with well-defined particle sizes, shapes and densities. Electron beam lithography allows the fabrication of particle arrays with precise geometrical parameters [6,7]. However, the minimum structure size is around 50 nm and ensembles with high particle density cannot be produced. Metal colloids with uniform size, synthesized in reverse micelles, are suited to form self-assembled two and three-dimensional supercrystals with high packing density [8–10]. The inter-particle distance is, however, hardly tunable in this approach and optical properties are altered by ligand shells surrounding the colloids. On the other hand, metal vapor deposition on a dielectric support offers a wide range of possibilities to manipulate size, shape and density of particles in an ensemble. Although a perfect particle arrangement on the surface is rarely achieved [11], particle densities are adjustable over few orders of magnitude when applying the right preparation conditions. Crucial parameters influencing particle geometry and density are the deposition temperature, the metal-atom flux and the presence of suited nucleation sites on the support. Various experiments using vapor-deposited Ag and Au particles have been reported in the literature, investigating the effect of particle size, shape [12–17], and inter-particle spacing [6,7,18] on the optical properties.

* Corresponding author. Tel.: +49 30 8413 4191; fax: +49 30 8413 4101.
E-mail address: nilius@fhi-berlin.mpg.de (N. Nilius).

0039-6028/$ - see front matter
doi:10.1016/j.susc.2006.03.010

In this work, we primarily focus on the influence of the particle density on plasmon excitations in ensembles of vapor-deposited Ag particles grown on Al_2O_3/NiAl(1 1 0). The study covers a density range between 0.5×10^{11} and 11×10^{11} cm^{-2}, while keeping the particle size and shape relatively constant. The combination of scanning tunneling microscopy (STM) and photon emission spectroscopy used in the experiment is particularly suited for a simultaneous topographic and optical characterization of a particle ensemble. By selecting the tip-sample distance, it enables investigation of well-defined sample areas, adjustable between several μm^2 and a few nm^2. The approach therefore avoids inhomogeneous spectral information, resulting from ill-defined and defect-rich sample areas. The technique was introduced by Berndt and Gimzewski to study the light emission from planar surfaces [19].

The experimental setup consists of an UHV–STM operated at 300 K, which is especially designed to investigate light emission from the tip-sample junction. For this purpose, a beetle-type microscope head is surrounded by a parabolic mirror to collect photons from the tunneling junction. A second mirror outside the vacuum chamber focuses the light onto the entrance slit of a grating spectrograph attached to a liquid-nitrogen cooled CCD detector [20]. A well-ordered alumina film of 5 Å thickness is used as substrate in the experiments. The film is prepared by oxidizing a clean NiAl(1 1 0) surface at 500 K, followed by annealing to 1000 K [5]. The atomically flat Al_2O_3 film is then exposed to a flux of Ag atoms from a Mo crucible heated via electron bombardment. Several methods are employed to control the particle density on the oxide surface, and to adjust the particle size and shape. Samples with low densities are obtained by silver deposition at elevated temperatures of up to 500 K. Cooling the sample to 200 K increases the nucleation density of Ag. Ensembles with even higher densities are prepared by bombarding the oxide surface with Ar^+ ions of 500 eV kinetic energy prior to Ag deposition. This procedure creates additional nucleation centers on the alumina film. In order to keep the mean particle size constant, the total Ag exposure is adapted to the particle density in the various preparations. Particle shapes could be controlled via the sample potential (V_{Sample}) with respect to the Ag doser (V_{Doser}) during evaporation. At equal potential, Ag atoms and a small fraction of Ag^+ ions created in the evaporation process arrive at the surface with thermal energy, which leads to the formation of dome-like particles. At negative sample potential (−800 V) with respect to the doser, Ag ions reach the surface with high kinetic energy, inducing changes in the Ag growth regime towards flat particles with disk-like shapes.

Fig. 1 shows STM topographic images of Ag particle ensembles with increasing density. Whereas particles in A–F have dome-like shapes ($V_{Sample} = V_{Doser}$), particles in G–I are more disk-like ($V_{Sample} = -800$ V). The particle density varies between 1.0×10^{11} and 8.0×10^{11} cm^{-2} in the preparations A–F, and between 3.5×10^{11} and 10×10^{11} cm^{-2} in G–I, respectively.[1] Silver growth on alumina follows the Volmer–Weber mode. The nucleation typically takes place at line defects, such as step edges and domain boundaries of the oxide film, yielding a number density of $\sim 2 \times 10^{11}$ cm^{-2} at 300 K. This value is modified by changing the sample temperature during deposition. At 200 K, the Ag diffusion length is not sufficient that all atoms reach a preferential binding site, and nucleation takes place also within Al_2O_3 terraces. At elevated temperatures (500 K) only deep traps such as step edges act as nucleation centers, leading to smaller particle densities but also to an inhomogeneous, chain-like particle distribution on the surface (Fig. 1A). The distribution becomes more uniform, when artificial nucleation sites are created by Ar^+ sputtering of the alumina film (Fig. 1D–F,H,I). The number of defects is controlled via the flux of incoming ions and saturates at a maximum density of 11×10^{11} cm^{-2}.

The distinct shape difference between dome-like and disk-like particles is shown in the height profiles of Fig. 2. Both particle types are prepared at similar experimental conditions except for the potential difference between sample and Ag doser during evaporation. Whereas dome-like particles are formed at zero potential difference, they become disk-like for high negative voltages applied to the sample. This behavior can be rationalized as follows. The electron-beam evaporator used in the experiment produces a small fraction of Ag^+ ions (0.5%) beside neutral Ag atoms. As long as doser and sample are on the same potential, the ions have no effect on the Ag growth regime, and particles form with equilibrium shape. The low silver-alumina adhesion energy and the large difference in surface-free-energy between metal and oxide strongly favors the formation of compact 3D particles with large aspect ratio [21]. On the other hand, the impact of high-energy Ag ions on a negatively biased sample perturbs the thermodynamic growth regime and leads to the formation of flat particles. Two effects have to be taken into account to explain this observation. First, Ag^+ sputtering locally destroys the oxide surface, inducing new nucleation sites with larger Ag–Al_2O_3 interaction strength. The increased metal-oxide adhesion shifts the equilibrium shape towards flat particles exhibiting [1 1 1] facets [22]. Secondly, the impact of Ag ions on already existing particles produces holes in their surface, which have to be filled with material from higher-lying particle regions. In the restructuring process, the particles successively flatten and form large [1 1 1] facets due to the low surface-free-energy of this crystallographic plane. The existence of [1 1 1] facets is deduced from the hexagonal shape of flat particles as seen in Fig. 1G.

Special care has been taken to produce particle ensembles with a relatively small size and shape distribution, in order to keep the particle density the only variable parameter in the experiment. Particle sizes were controlled by

[1] Particle densities in the experiment correspond to 2D filling factors ($A_{Particles}/A_{Surface}$), ranging between 0.02–0.50 for dome-like and 0.20–0.80 for disk-like ensembles.

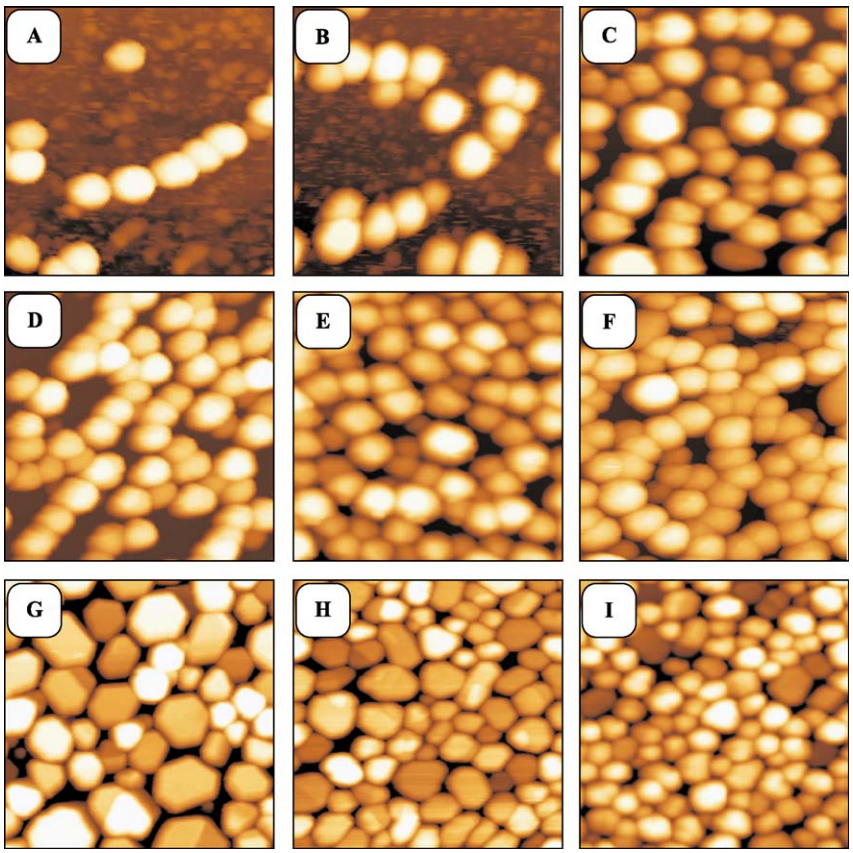

Fig. 1. STM topographic images of Ag particles on Al_2O_3/NiAl(1 1 0), ($V_{sample} = 1$ V, $I = 0.05$ nA). The particle density increases from 1.0×10^{11} to 8.0×10^{11} cm^{-2} in A–F, and from 3.5×10^{11} and 10.5×10^{11} cm^{-2} in G–I. While particles in (A–F) have predominately dome-like shapes, particles in (G–I) are more disk-like. Image sizes are 100×100 nm^2.

adjusting the total Ag exposure to the number density. Fig. 3 shows a summary of measured heights for dome-like (closed symbols) and disk-like (open symbols) particles from different preparation procedures. Each data point is an average of approximately 25 single-particle measurements. Particle diameters have been determined from the total Ag coverage and experimental particle heights, assuming a truncated ellipsoidal shape.[2] Whereas dome-like particles are rather uniform in size, the size distribution of disk-like particles is comparatively large. The average particle height and diameter for both shapes slightly decrease with increasing particle density, however, the aspect ratio remains relatively constant over the full density range. Dome-like particles are characterized by a height-to-radius ratio of ~0.55; disk-like ones have an aspect ratio of ~0.3.

The effect of particle–particle interactions on the optical properties is investigated by exciting an Ag particle ensemble with field-emitted electrons from the STM tip and detecting the photon emission from the tip-sample junction. For this purpose, the tip is retracted from the surface until a field emission current of 1 nA is stabilized for −240 V tip bias. The field-emitted electrons spread over a wide surface area of roughly 100.000 nm^2 and coherently excite the particle ensemble. Electron injection into the sample is limited to 60 s per spectrum to avoid structural damage of the surface. Normalized photon emission spectra from dome- and disk-like Ag particle ensembles with increasing density are shown in Fig. 4. The spectra are dominated by a pronounced emission line between 330–355 nm, attributed to the radiative decay of Mie plasmons excited by the electron injection [13,23]. The Mie plasmons in isolated metal spheres are three-fold degenerated in energy and determined by particle size, material and dielectric environment. The degenerated mode splits due to non-spherical particle shapes and dipole–dipole coupling with neighboring particles [1]. In principle, two plasmon modes should be observed for supported nano-particles, corresponding to plasmon oscillations parallel (1, 1) and perpendicular (1, 0) to the support. The single emission peak in the spectra of Fig. 4 is assigned to the (1, 0) plasmon, as this mode is preferentially excited by field-emitted electrons injected along the surface normal [10]. In addition, the photon detection system used in the experiment is more sensitive to light emitted from the (1, 0) plasmon. The mode assignment is in correspondence to results reported earlier for Ag particle ensembles on various supports including

[2] The coverage was calibrated by dosing Ag onto clean NiAl(1 1 0), where it grows in a layer-by-layer fashion and the amount can directly be determined from STM images.

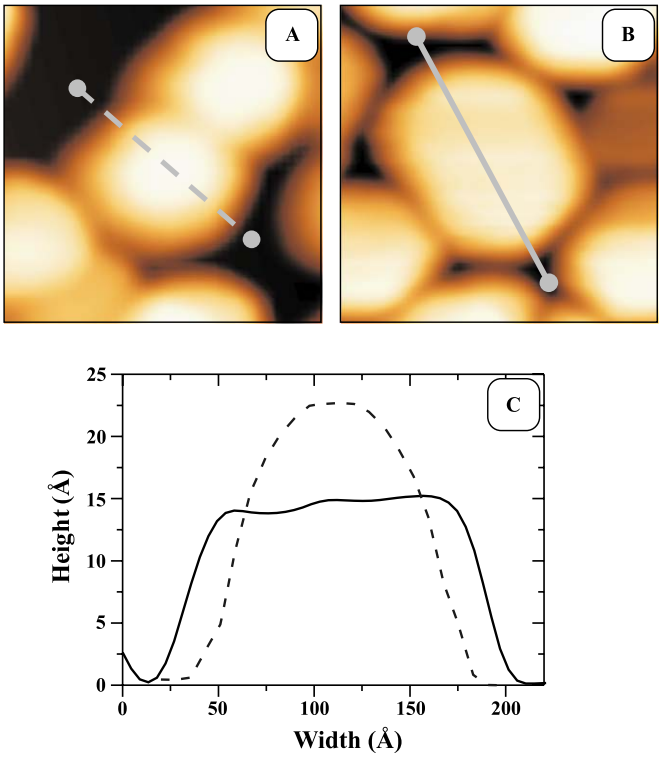

Fig. 2. STM topographic images of (A) a dome-like and (B) a disk-like Ag particle on Al_2O_3/NiAl(1 1 0) (25×25 nm^2). (C) Height profiles of particles shown in (A) and (B). Particle diameters are not corrected for tip convolution effects and represent therefore upper limits of the real size.

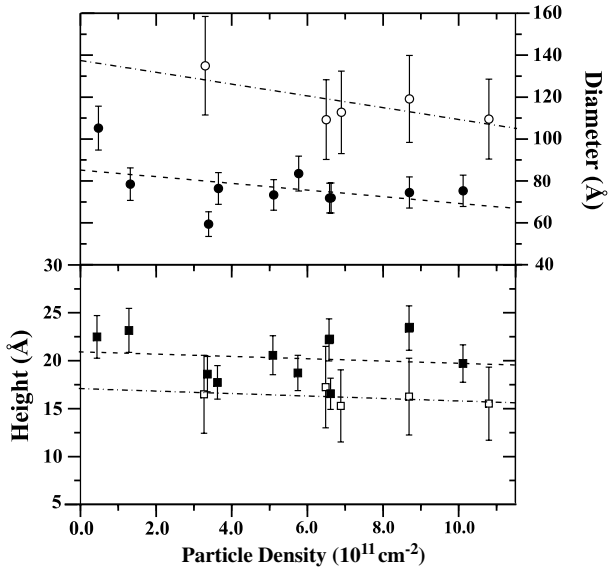

Fig. 3. (Lower part) Average height of dome-like (closed symbols) and disk-like (open symbols) Ag particles for different particle densities, as deduced from STM topographic images. Solid lines are guides to the eye. (Upper part) Average diameters of dome-like (closed symbols) and disk-like (open symbols) Ag particles, derived from experimental particle heights and the total Ag coverage on the surface.

amorphous alumina [1,12,16]. For dome-like particles, a distinct blue shift of the (1,0) plasmon peak is observed with increasing particle density, from 354 ± 2 nm (3.50 eV) for 0.5×10^{11} particles per cm^{-2} to 338 ± 2 nm (3.66 eV) for a density of 10×10^{11} cm^{-2} (Fig. 4A). For disk-like particles, peak positions are generally higher in energy (330 ± 2 nm or 3.75 eV), and exhibit almost no shift with particle density (Fig. 4B). The evolution of the (1,0) mode energy as a function of density is summarized in Fig. 5. When evaluating these results, the rather inhomogeneous distribution of Ag particles at densities below 3.0×10^{11} cm^{-2} has to be taken into account. At low densities, the concentration of particles along step edges and oxide line defects results in a locally enhanced coupling strength (Fig. 1A). Representative data on the ensemble interactions are obtained at higher densities, where particles are more homogeneously distributed.

As the mean size and shape of Ag particles were kept constant in all preparations discussed here, the shift in plasmon energy is mainly attributed to the effect of dipole–dipole interactions in the particle layer. Electromagnetic coupling affects the (1,0) and (1,1) plasmon modes in opposite manner [1,10]. Dipole oscillations in the substrate plane experience constructive interference, which shifts the (1,1) mode to lower energies with increasing density. The out-of-plane (1,0) dipoles on the other hand interfere destructively, leading to an energy rise with increasing particle density. The observed blue-shift of the emission peak for dome-like particles reflects these enhanced dipole interactions, and supports its assignment to the (1,0) Mie plasmon. The interaction energy between two isolated dipoles follows a d^{-3} dependence on the dipole–dipole distance d, but falls off slower for a 2D array of out-of-plane dipoles. The experimental data for dome-like particles can be reproduced with a $d^{-1.8}$ dependence (Fig. 5, dotted line). The red shift of the (1,1) and the blue shift of the (1,0) plasmons with increasing density have earlier been observed for lithographically fabricated particle ensembles [6,7,24]. Particle sizes and inter-particle separations in those experiments were in the order of the wavelength of light and demanded an interpretation of the optical data in the framework of retardation and multi-pole effects, whereas a treatment within the dipole approximation is sufficient here. For lithographically prepared ensembles, a shift of the (1,0) mode of roughly 50 meV was found, when changing the separation-to-diameter ratio of the particles from 3 to 1. Due to smaller particle sizes, the blue shift for dome-like particles is considerably reduced in our experiment (15 meV).

The absent shift of the (1,0) Mie plasmon for disk-like particles as a function of density is related to two facts (Fig. 5). First, the (1,0) mode in flat particles is characterized by a small oscillator strength compared to round particles with the same volume, because of the shorter (1,0) dipole lengths. Consequently, the coupling efficiency between neighboring out-of-plane dipoles is reduced with respect to dome-like ensembles and the blue shift is smaller. Second, the low aspect ratio of disk-like particles already yields relatively high (1,0) mode energies, independent of the particle density. The upper energy limit for a Mie plasmon is given by the position of the surface plasmon in a

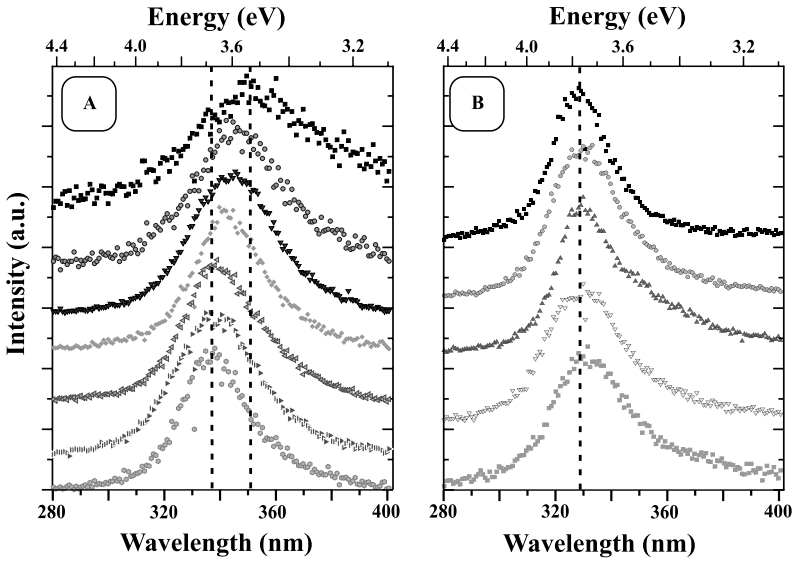

Fig. 4. Normalized photon emission spectra for (A) dome-like and (B) disk-like Ag particles on Al_2O_3/NiAl(1 1 0). The particle density increases from the top to the bottom, in (A) from 0.5×10^{11} to 10×10^{11} cm^{-2} and in (B) from 3.5×10^{11} to 11×10^{11} cm^{-2}. All spectra are recorded at a tip bias of −240 V and an electron current of 1 nA.

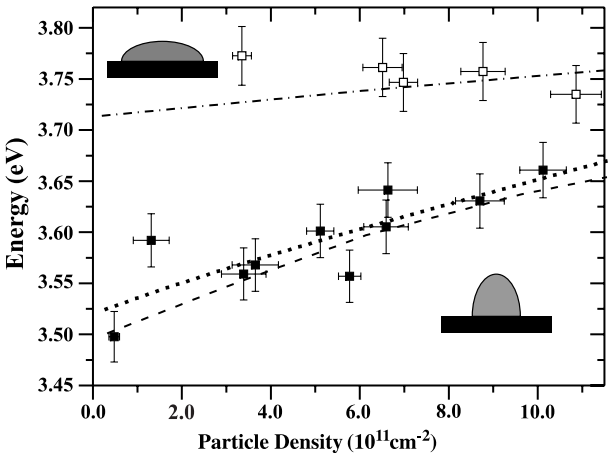

Fig. 5. Dependence of the plasmon energy on the particle density for ensembles of dome-like (closed squares) and disk-like (open squares) Ag particles. The dotted line fits the experimental data to a power law, relating the dipole–dipole interaction energy E to the mean particle separation d by: $E(d)\propto d^{-\alpha}$ with $\alpha=1.8$. Dashed and dash-dotted lines show the density dependence for dome and disk-like particle shapes, as calculated with the GranFilm program [25].

continuous silver film, which is located at ~3.76 eV [23]. When destructive dipole–dipole coupling pushes the plasmon energy towards this limit, the blue-shift of the Mie mode vanishes, as observed for disk-like particle ensembles.

Our qualitative interpretation of the experimental results is supported by model calculations on optical properties of dome and disk-like particles, performed with the GranFilm program. The code was written by R. Lazzari and I. Simonsen [25] and permits the determination of the polarizability of supported particles by solving the Maxwell equations. Optical absorption spectra of Ag particles on an Al_2O_3 substrate are calculated for varying densities using experimentally determined dielectric functions [26]. The particle distribution on the surface is described by the mean field approach, inter-particle interactions are included within the dipole approximation. The particles are modeled as truncated spheroids, determined by a perpendicular ($r_\perp$) and a parallel radius ($r_\parallel$) corresponding to the experimental particle height and radius, respectively. Dome-like particles are hence characterized by $r_\perp > r_\parallel$, while $r_\perp < r_\parallel$ accounts for disk-like shapes. Several combinations of radii have been tested in order to reproduce the experimental results, however, optimal fitting of the measured plasmon shift was possible only for a narrow range of radii. Reproduction of the data for dome-like particle ensembles is achieved by setting the particle geometry to $r_\perp = 46$ Å and $r_\parallel = 32$ Å (Fig. 5-dashed line). The calculated density dependence follows quantitatively the experimental behavior, emphasizing the dominant role of dipole–dipole interactions for the observed blue shift of the plasmon mode. For flat particle ensembles, the fitting procedure yields the following radii: $r_\perp = 27$ Å and $r_\parallel = 40$ Å. The agreement is not as good as for dome-shaped particles (Fig. 5 – dash-dotted line). While almost constant plasmon energy is observed experimentally, it somewhat blue shifts with increasing density in the calculations. The deviation might be related to a slightly larger aspect ratio for flat particles at higher density, which lowers the (1,0) Mie energy and thus compensates the blue-shift due to increased dipole interactions.

When comparing experimental and theoretical particle radii, we notice an overestimation of the theoretical particle height $r_\perp$ by almost a factor of two. This effect can be attributed to the neglect of the NiAl support below the Al_2O_3 film in the model. Dipole oscillations in the Ag particles induce pronounced image dipoles in the NiAl across the oxide film, which couple constructively to the (1,0)

plasmon mode. The resulting increase of the total dipole moment causes intensified interactions between the out-of-plane dipoles in neighboring particles. To judge the importance of this effect, we have placed the Ag particles directly on the NiAl support. Fitting this model to the experimental density dependence of the plasmon energy leads to a much better agreement between calculated and measured particle shapes. The fitted particle heights, $r_\perp = 33$ Å for dome-like and $r_\perp = 20$ Å for disk-like particles, are now comparable with the experimental values. However, line widths and energy positions of the Mie plasmon deviate more for a NiAl than a Al_2O_3 support, emphasizing that optical properties of the particle layer are influenced by the oxide film and the metal substrate as well.

In conclusion, we have studied electromagnetic interactions in Ag particle ensembles on Al_2O_3/NiAl(1 1 0) as a function of particle density, employing photon emission spectroscopy with the STM. Preparation parameters have been adjusted to vary the number density on the surface over a wide range, while keeping the particle geometry approximately constant. The optical spectra of so-prepared ensembles are dominated by (1,0) Mie plasmon excitations. For dome-shaped particles, the Mie mode shows a distinct blue shift with increasing particle density, attributed to destructive coupling of out-of-plane dipoles in the particle layer. For disk-like particles nearly constant plasmon energies are detected, manifesting the reduced influence of dipole–dipole interactions for extremely flat particles. The experiments demonstrate the possibility to tune the optical properties of Ag particle ensembles exclusively by changing the inter-particle separation.

References

[1] U. Kreibig, W. Vollmer, Optical Properties of Metal Clusters, Springer Series Materials Science, vol. 25, Springer, Berlin, 1995.

[2] K. Kneipp, Y. Wang, H. Kneipp, L.T. Perelman, I. Itzkan, R.R. Dasari, M.S. Feld, Phys. Rev. Lett. 78 (1997) 1667.

[3] Y. Dirix, C. Bastiaansen, W. Caseri, P. Smith, Adv. Mater. 11 (1999) 223.

[4] S.A. Maier, P.G. Kik, H.A. Atwater, S. Meltzer, E. Harel, B.E. Koel, A.A.G. Requicha, Nat. Mater. 2 (2003) 229.

[5] H.-J. Freund, M. Bäumer, H. Kuhlenbeck, Adv. Catal. 45 (2000) 333; K. Watanabe, Y. Matsumoto, M. Kampling, K. Al-Shamery, H.-J. Freund, Angew. Chem. 38 (1999) 2192.

[6] C.L. Haynes, A.D. McFarland, L. Zhao, R.P. Van Duyne, G.C. Schatz, L. Gunnarsson, J. Prikulis, B. Kasemo, M. Käll, J. Phys. Chem. B 107 (2003) 7337.

[7] W. Rechberger, A. Hohenau, A. Leitner, J.R. Krenn, B. Lamprecht, F.R. Aussenegg, Opt. Commun. 220 (2003) 137.

[8] L. Motte, F. Billoudet, M.P. Pileni, J. Phys. Chem. 99 (1995) 16425.

[9] M.P. Pileni, Nat. Mater. 2 (2003) 145.

[10] N. Nilius, H.-M. Benia, C. Salzemann, G. Rupprechter, A. Brioude, M.-P. Pileni, H.-J. Freund, Chem. Phys. Lett. 413 (2005) 10.

[11] C. Becker, A. Rosenhahn, A. Wiltner, K. Bergmann, J. Schneider, P. Pervan, M. Milun, M. Kralj, K. Wandelt, New J. Phys. 4 (2002) 75.1.

[12] T. Wenzel, J. Bosbach, F. Stietz, F. Träger, Surf. Sci. 432 (1999) 257.

[13] N. Nilius, N. Ernst, H.-J. Freund, Phys. Rev. Lett. 84 (2000) 3994.

[14] J.J. Mock, M. Barbic, D.R. Smith, D.A. Schultz, S. Schultz, J. Chem. Phys. 116 (2002) 6755.

[15] T. Wenzel, J. Bosbach, A. Goldmann, F. Stietz, F. Trager, App. Phys. B 69 (1999) 513.

[16] D. Martin, J. Jupille, Y. Borensztein, Surf. Sci. 402 (1998) 433.

[17] A. Hilger, M. Tenfelde, U. Kreibig, Appl. Phys. B 73 (2001) 361.

[18] Y. Lu, G.L. Liu, L.P. Lee, Nano Lett. 5 (2005) 5.

[19] R. Berndt, in: R. Wiesendanger (Ed.), Scanning Probe Microscopy, Springer, Berlin, 1998, p. 97.

[20] N. Nilius, A. Cörper, G. Bozdech, N. Ernst, H.-J. Freund, Prog. Surf. Sci. 67 (2001) 99.

[21] C. Noguera, Physics and Chemistry at Oxide surfaces, University Press, Cambridge, 1996, p. 128.

[22] G. Wulff, Ze. Kristallogr. 34 (1901) 449.

[23] J.W. Little, T.A. Callcott, T.L. Ferrell, E.T. Arakawa, Phys. Rev. B 29 (1984) 1606.

[24] K.-H. Su, Q.-H. Wei, X. Zhang, J.J. Mock, D.R. Smith, S. Schultz, Nano Lett. 3 (2003) 1087.

[25] R. Lazzari, I. Simonsen, Thin Solid Films 419 (2002) 124.

[26] E.D. Palik (Ed.), Handbook of Optical Constants of Solids, Academic Press, Orlando, 1985.